

# Natural Magnetite for thermal energy storage: Excellent thermophysical properties, reversible latent heat transition and controlled thermal conductivity



Yaroslav Grosu\*, Abdessamad Faik, Iñigo Ortega-Fernández, Bruno D'Aguanno

CIC Energigune, Albert Einstein 48, Miñano, Álava 01510, Spain

## ARTICLE INFO

**Keywords:**

Concentrated solar power  
Thermal energy storage  
Thermocline storage system

## ABSTRACT

Thermal energy storage (TES) has gained growing interest in the area of renewable energy due to its great potential for increasing the efficiency of concentrated solar power (CSP) plants. One of the central issues is the development of a working body with desirable properties, namely, thermal conductivity; heat capacity; density; price; availability; and eco-friendliness. This study reports the thermophysical characterization and proposes a reliable and industrial appropriate treatment route for natural Magnetite to obtain a material possessing not only a combination of the above properties, but also the possibility of easy control (programming) of thermal conductivity in a wide range of values. The combination of such properties is exceptional and crucially advantageous for TES applications like packed-bed heat storage systems.

## 1. Introduction

Magnetite ( $\text{Fe}_3\text{O}_4$ ) is a prominent natural material whose properties have attracted attention since antiquity. Its usage for practical applications has been documented due to its magnetic properties as far back as the 8th century [1]. Today, the range of applications is impressive ranging from drug delivery, magnetocytolysis [2], and magnetic resonance imaging [3,4] to cancer therapy [5], hyperthermia [6], nanocomposites, ferrofluids [7,8] and more [9]. Magnetite has many advantages such as availability, low cost, ecological friendliness and non-flammability, yet it has been mentioned only briefly as a potential material for Thermal Energy Storage (TES) [10] as well as part of iron ore [11]. Furthermore, it has not been studied extensively for TES applications perhaps due to its low thermal conductivity, which is a critical property in this field. On the other hand, the iron oxide, Hematite ( $\alpha\text{-Fe}_2\text{O}_3$ ), noted to have much higher thermal conductivity, was used as part of composite TES materials such as concrete [12,13] and the composites consist of natural materials [14]. It is indicated in [12,13] that iron oxide is used, however, considering that it is obtained as by-product from strip steel production it is a reasonable assumption that it is Hematite. In this paper, we propose a simple treatment route for natural Magnetite for beneficiation from high and controlled thermal conductivity and increased energy density due to reversible antiferromagnetic phase transition. This would provide a cheap, largely available, ecologically friendly material with excellent and tunable

thermophysical properties for TES applications, particularly for packed-bed thermocline storage systems, which have received considerable attention as a promising new TES configuration [15–18] using different combinations of heat transfer fluids with or without TES materials as air with alumina [15,16] or steatite in [18], Hitec molten salt in [19] and thermal oil with pebble in [20].

TES is highly topical due to its great potential for increasing the efficiency and to level off daily demand and supply of Concentrated solar power (CSP) plants [21–23]. The simple concept that excess heat present at CSP plants during sunlight hours can be stored and transformed into electricity during night time or cloudy periods, raises challenging ensemble of requirements for the properties of TES materials: thermal conductivity, high heat capacity and density, excellent stability, compatibility with HTF in the operation temperature range, non-flammability, non-toxicity, availability and low cost. The latter in particular is becoming a crucial parameter for reaching high competitiveness in the field of renewable energy [23].

Apart from thermo-chemical energy storage systems, there are two main methods for storing heat [21,22]: (i) by means of a heating-cooling cycle which takes advantage of materials with high heat capacity – sensible heat storage; and (ii) by taking advantage of the enthalpy of reversible phase transitions of different nature, which are associated with additional heat supply to the material upon heating and its release upon cooling – latent heat storage. Today, materials with heat capacity in the range of 0.5–2.0 J/K g are considered acceptable

\* Corresponding author.

E-mail addresses: [ygrosu@cicenergigune.com](mailto:ygrosu@cicenergigune.com) (Y. Grosu), [aafaik@cicenergigune.com](mailto:aafaik@cicenergigune.com) (A. Faik).

for sensible TES.

Typically, thermal conductivity plays a major role in obtaining an efficient steep thermocline system. While higher values are beneficial during charging and discharging periods, lower values are preferential for maintaining a steep thermocline zone to avoid its deterring during idle periods. For these reasons, optimum value may sometimes be required for each specific packed-bed system [24].

The values of thermal conductivity are reported in the range of 0.3–100 W/K m [25–28] and whilst very high values are reported for expensive or rare materials, the thermal conductivity is rarely higher than 5 W/K m for low-cost materials [25–28].

In this paper, an evaluation of Magnetite for a new area of application – Thermal Energy Storage – is investigated taking advantage of its excellent thermophysical properties for sensible TES combined with exceptional ability to simply program its thermal conductivity in a wide range of values and, additionally, benefit from the latent heat related to its antiferromagnetic transition at high temperature. Considering the aforementioned advantages of natural Magnetite, it may be considered as a very promising candidate for TES applications, especially for packed-bed systems, in a wide temperature range (up at least to 1000 °C).

## 2. Methods

### 2.1. Material

Natural Magnetite used in this work was supplied by LKAB minerals company (Sweden). The raw material and samples treated in the furnace at 400, 800 or 1000 °C for 1–21 days under air atmosphere were investigated. The material is presented in pebbles of approximately 1 cm<sup>3</sup>. The names of the samples corresponding to the particular conditions of treatment are presented in Table 1. The raw Magnetite-p powder sample was obtained by graining the raw Magnetite bulk material. The Magnetite 1000-p powder sample was obtained by 1000 °C treatment of raw Magnetite-p powder for 1 day. The size of the grains of the powder sample was in the order of tenth of microns, which was verified by SEM technique.

### 2.2. Characterization techniques and methodology

#### 2.2.1. Inductively coupled plasma – optical emission spectroscopy (ICP-OES)

The chemical composition of the Magnetite was studied by ICP-OES with a Perkin Elmer Optima 2000 OV. For these measurements, fine powder of the sample was obtained and fused with 99.9% lithium metaborate in high purity graphite crucibles and later dissolved with diluted HNO<sub>3</sub> (trace metal grade nitric acid and ultrapure Milli-Q®

**Table 1**

Treatment conditions for different samples of Magnetite.

Sample name	Treatment time (days)	Treatment temperature (°C)	Form
Raw Magnetite	–	–	Bulk
Raw Magnetite-p	–	–	Powder
Magnetite 400	1	400	Bulk
Magnetite 800	1	800	Bulk
Magnetite 1000-p	1	1000	Powder
Magnetite 1000-1	1	1000	Bulk
Magnetite 1000-2	2	1000	Bulk
Magnetite 1000-7	7	1000	Bulk
Magnetite 1000-21	21	1000	Bulk

**Table 2**

Chemical composition of temperature treated Magnetite obtained by ICP technique.

Compound (%)							
Fe <sub>2</sub> O <sub>3</sub>	SiO <sub>2</sub>	MgO	Al <sub>2</sub> O <sub>3</sub>	K <sub>2</sub> O	Na <sub>2</sub> O	MnO	CaO

D.L. is detection limit.

water were used to prepare the dissolution). The solution obtained was directly analyzed by using the accepted standard practice reported in ref. [29], which includes high-temperature treatment. The analysis was carried out for the major and trace elements (Al, Ca, Fe, Mg, Mn, Si, Na and K).

#### 2.2.2. Scanning electron microscopy (SEM)

The samples were imaged by means of a Quanta 200 FEG scanning electron microscope operated in high vacuum mode at 30 kV and with a back scattered electron detector (BSED). In addition, energy-dispersive X-ray spectroscopy (EDX) analyses were carried out in order to obtain chemical composition maps of the different observed samples zones.

#### 2.2.3. X-ray power diffraction (XRD)

X-ray powder diffraction technique was used for the structural analysis by means of a Bruker D8 Advance X-ray diffractometer equipped with a LYNXEYE detector using CuK $\alpha$  radiation ( $\lambda=1.5418 \text{ \AA}$ ) and  $0\text{--}2\theta$  geometry. Data were collected at room temperature between 25° and 80° in  $2\theta$  with a step size of 0.02° and counting time of 8 s per step. The EVA program was used to determine the phase composition of the material.

#### 2.2.4. Densitometry

Bulk and skeletal densities were measured using cubical samples of around 10 mm side length. A high-precision balance and caliber were used to calculate the apparent density while the helium pycnometer AccuPyc II 1340 from Micromeritics was used to determine the skeletal density.

#### 2.2.5. Differential scanning calorimetry (DSC)

The heat capacity ( $C_p$ ) of the investigated materials was measured in the 25–500 °C temperature range by the DSC technique (Thermal Analysis Q2000 model) using the modulated heating ramp dynamic method [30], which allows a direct measurement of the  $C_p$ . The modulation amplitude and period have been fixed to  $\pm 1 \text{ K}$  and 120 s, respectively. The selected continuous heating rate was 2 K/min. The instrument was previously calibrated using sapphire as standard material. Around 25 mg of bulk samples, previously polished to ensure a good thermal contact, were placed inside high-conductive aluminum holder sample which then were hermetically closed. The experimental error of this technique is below 3%.

The enthalpy of phase transition was measured in the 25–710 °C temperature range with the same apparatus using the standard DSC approach.

#### 2.2.6. Laser Flash Apparatus (LFA)

The thermal conductivity ( $\lambda$ ) values were obtained in indirect way from the thermal diffusivity ( $\alpha$ ), density ( $\rho$ ) and heat capacity ( $C_p$ ), according to the following equation:  $\lambda=\alpha \cdot \rho \cdot C_p$ .

The thermal diffusivity of the studied materials was obtained by using the Laser Flash Apparatus (LFA) method [31], using a LFA-457 from NETZSCH. Square samples with a side length of 10 mm and a thickness of 2 mm were used. In order to minimize the experimental error, a graphite film prime was added over the samples and the reference surfaces.

LFA technique was also used for indirect  $C_p$  measurement of

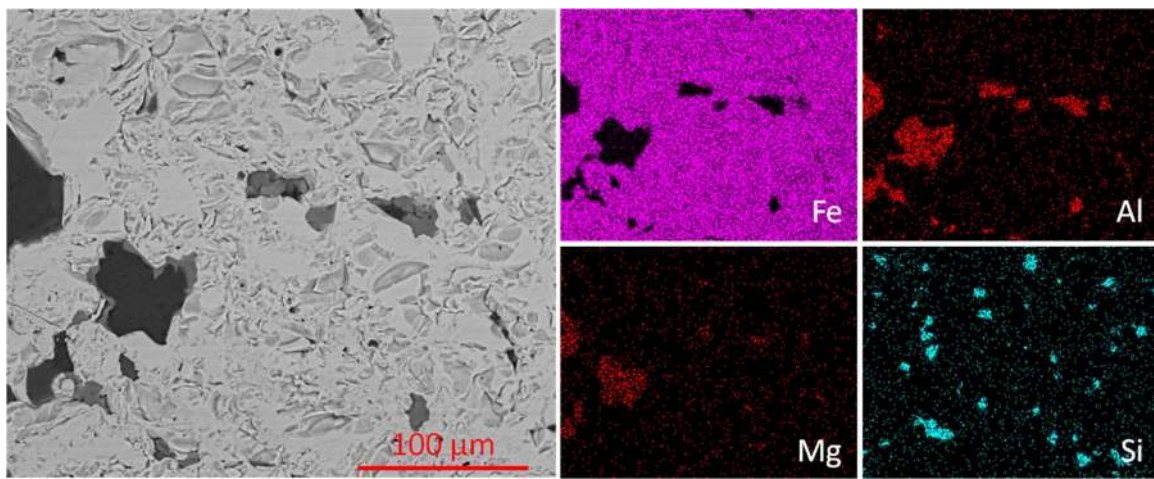


**Fig. 1.** SEM image and EDX mapping of Magnetite.

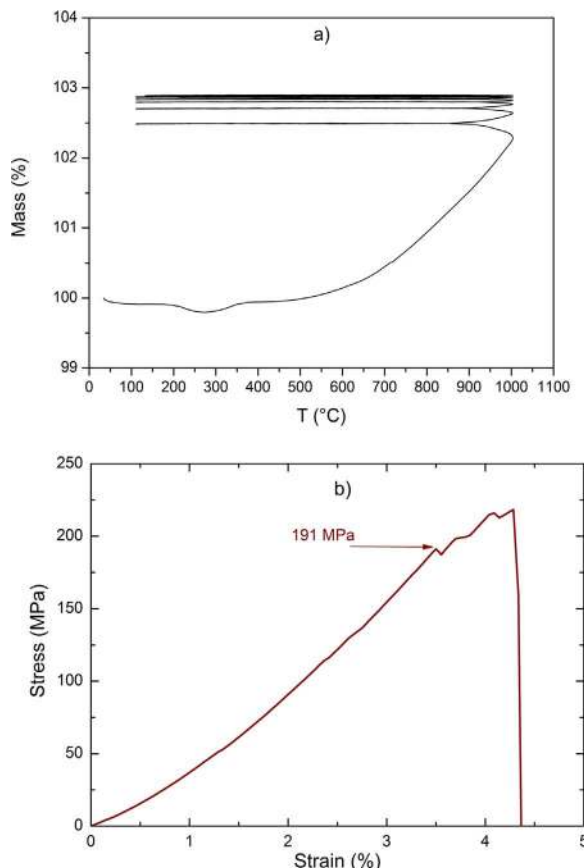


**Fig. 2.** Thermal and mechanical stability of the raw Magnetite: a) TGA curve of seven thermal cycles of raw Magnetite-p and b) mechanical strength measurement for raw Magnetite at room temperature.

Magnetite sample in the 25–1000 °C temperature range. The LFA  $C_p$  experimental data were determined by a comparative heat capacity determination method, where the investigated Magnetite sample and a reference material (in this case pyroceram®) were measured subsequently under the same conditions. The heat capacity of the sample was calculated according to the following equation:

$$c_p^{\text{Sample}} = \frac{T^{\text{Ref}}}{T^{\text{Sample}}} \cdot \frac{(\rho \cdot l)^{\text{Ref}}}{(\rho \cdot l)^{\text{Sample}}} \cdot c_p^{\text{Ref}},$$

where  $T$  is the temperature and  $l$  is the thickness of the Magnetite and reference sample. The experimental error of this technique is below 5%

[32].

#### 2.2.7. Physical properties measurement system (PPMS)

Saturation magnetization measurements were carried out in a Quantum Design MPMS SQUID magnetometer at room temperature in the 0–3 T range at 1000 Hz and  $10^{-3}$  T amplitude.

#### 2.2.8. Thermogravimetric analysis (TGA)

Thermogravimetric analysis of the raw Magnetite-p was carried out by using a thermal analyser NETZSCH STA 449 F3 Jupiter. The measurements were conducted in a compressed air flow of 60 ml/min in order to study the thermal stability of the sample. Seven cycles between room temperature and 1000 °C at a heating/cooling rate of 10 °C/min were carried out.

#### 2.2.9. Mechanical strength test

For the compression tests, the samples of the specific size of 10 mm×10 mm×10 mm were prepared. The compression tests were carried out by using Universal Machine INSTRON 4206 at room temperature (RT) with a test speed of 3 mm/min and load cell of 100 kN. The compressive yield strength ( $\sigma$ ) was calculated as  $\sigma=F/A$ , where  $F$  is the load at yield, and  $A$  is the cross-section area.

### 3. Results and discussion

#### 3.1. Chemical composition and structural characterization

The chemical composition of the studied Magnetite measured by ICP-OES technique is given in Table 2, where obtained concentrations of the cations are given as oxides. It is important to note that preparation of the sample according to ref. [29] requires temperature treatment of the powder sample at high temperatures reaching 1000 °C. For that reason we speak here about temperature treated and oxidized sample of Magnetite – Hematite, which will be discussed in more detail below.

From Table 2 it can be seen that used Magnetite has rather high-purity for a natural material and is mostly presented by iron oxide, with impurities consisting mainly of Al, Si and Mg.

SEM images as well as EDX mapping of the raw Magnetite are presented in Fig. 1. It can be clearly observed that this material is mainly formed by big iron oxide crystals (bigger than 100 μm) which are typical of Magnetite rocks.

In order to check the thermal stability of Magnetite, TGA measurements were performed in air atmosphere for powder raw Magnetite (raw Magnetite-p). From the Fig. 2a it is clearly seen that upon first heating, there is mass gain for the raw Magnetite-p, which decreases

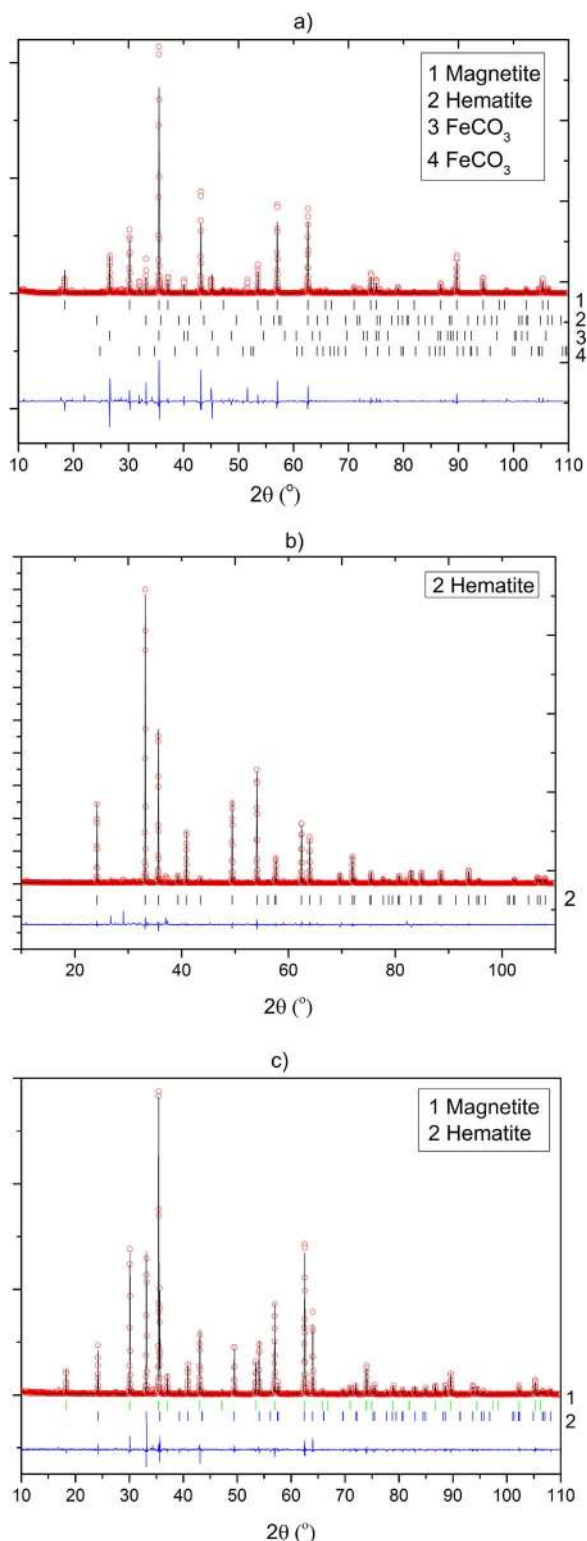


**Fig. 3.** XRD patterns of a) raw Magnetite, b) Magnetite 1000-p, c) Magnetite 1000-21. Red circles are for measured values, black lines are for calculated pattern, blue lines are differences curves and sticks are for Bragg peaks. (For interpretation of the references to color in this figure legend, the reader is referred to the web version of this article.)

with successive cycling and reaches saturation after the third cycle. Such mass variation is most probably due to the sample oxidation from Magnetite  $Fe_3O_4$  to Hematite  $\alpha-Fe_2O_3$ . There is also a small mass decrease in 200–300 °C, which seems to be related to iron carbonate decomposition, which may be seen from the XRD analysis provided below. In order to check mechanical stability of the material mechan-

**Table 3**

Degree of transformation of Magnetite to Hematite with time in the bulk sample treated at 1000 °C.

Treatment time (days)	XRD		PPMS	
	Magnetite (%)	Hematite (%)	Magnetite (%)	Hematite (%)
0	99	1	100	0
2	73	27	73	27
7	59	41	56	44
21	60	40	61	39

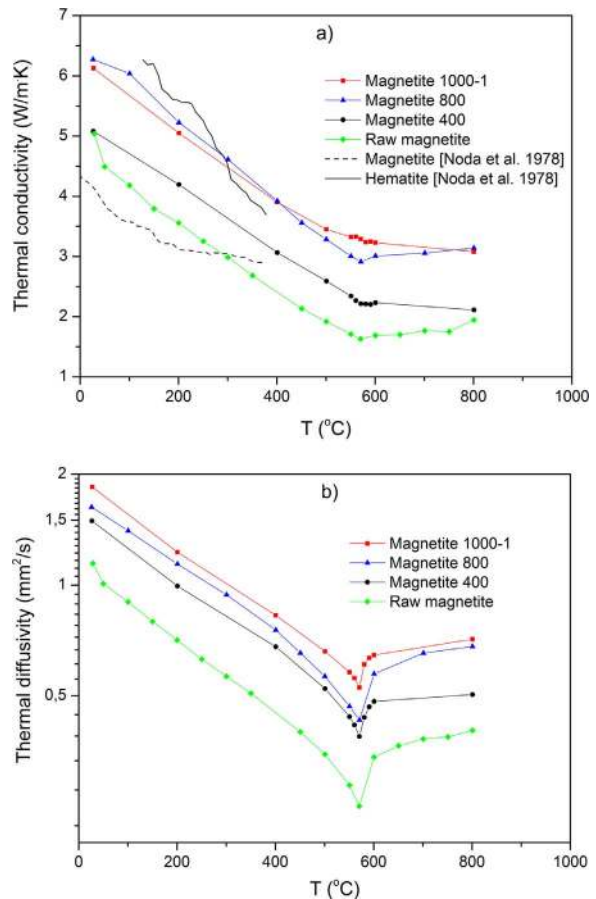


**Fig. 4.** a) Thermal conductivity and b) thermal diffusivity of the Magnetite depending on the treatment temperature.

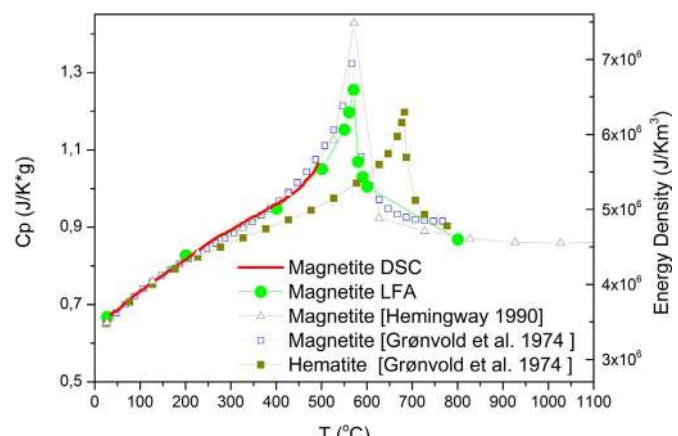


**Fig. 5.** Heat capacity and energy density of Magnetite 1000-1 measured by DSC and LFA techniques.

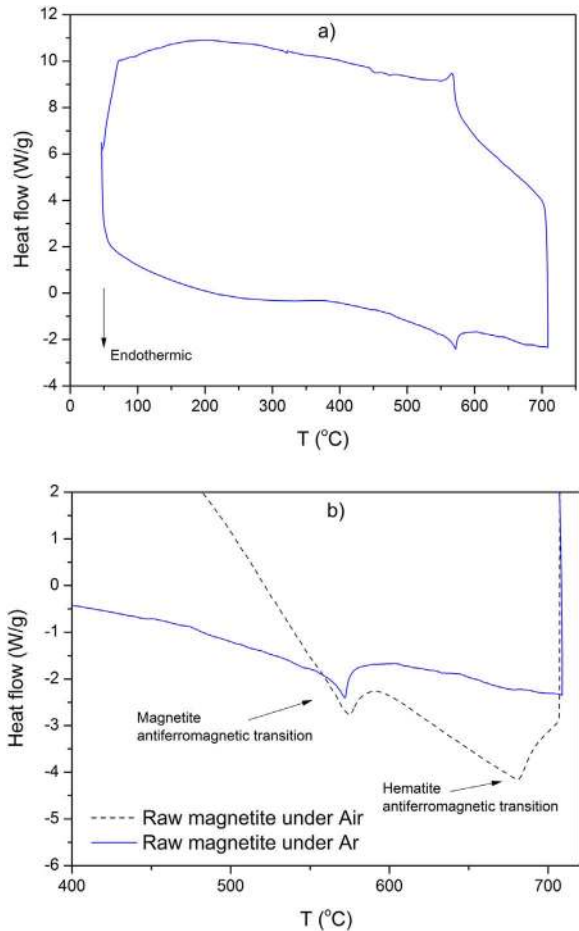


**Fig. 6.** a) 25th DSC cycle for raw Magnetite (bulk piece) under air atmosphere. b) 25th DSC cycle for raw Magnetite-p (powder) at air atmosphere.

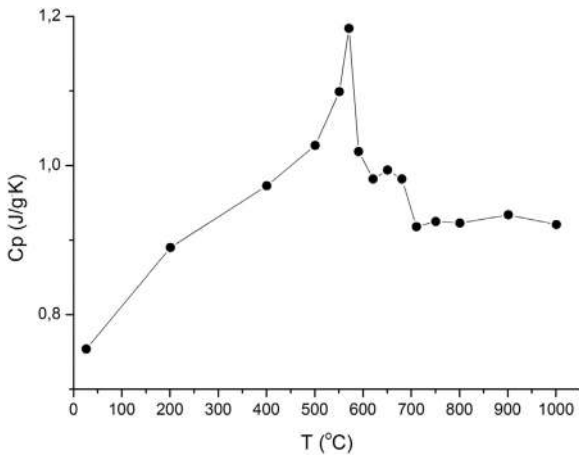


**Fig. 7.** LFA measurement for Magnetite 1000-21 sample.

ical strength test was performed for raw Magnetite at room temperature revealing that at 191 MPa some cracking appears (Fig. 2b), and the material collapses completely at 218 MPa. Such observation reveals a good mechanical properties and ability of this material to sustain high load in packed-bed configuration.

XRD Patterns of Magnetite treated at different conditions are presented in Fig. 3.

The raw material corresponds to Magnetite ( $Fe_3O_4$ ) with some impurities presented by iron carbonate (Fig. 3a). The amount of Hematite present in the raw material is negligible. Whilst the 1000 °C treated powder of Magnetite (Magnetite 1000-p) is completely

oxidized to Hematite (Fig. 3b), at the same time, the sample treated as a bulk piece for 21 days at 1000 °C (Magnetite 1000-21) shows preservation of large amounts of Magnetite (60%) and only partial oxidation to Hematite (40%). This is most probably due to limited diffusivity of oxygen into the bulk piece of material (Fig. 3c). The XRD quantitative analysis of such partial oxidation depending on the time of high temperature treatment at 1000 °C is summarized in Table 3.

It can be seen that for the investigated material after 2–7 days treatment at 1000 °C the saturation is reached in the Magnetite to Hematite transformation process and further treatment does not increase the Hematite content.

Additionally, the PPMS technique was used to quantify the ratio between Magnetite and Hematite upon temperature treatment. By using well known values of saturation magnetization of Magnetite ( $M_S^{Fe_3O_4}$ ) and Hematite ( $M_S^{Fe_2O_3}$ ) and measuring this property for the sample ( $M_S^{sample}$ ) the concentration of the Magnetite ( $x$ ) and Hematite ( $1 - x$ ) was found using the following equation:

$$x \cdot M_S^{Fe_3O_4} + (1 - x) \cdot M_S^{Fe_2O_3} = M_S^{sample}$$

A good agreement between the results from XRD and PPMS techniques is obtained (Table 3).

After temperature treatments of the material at 400, 800, 1000 °C, the corresponding densities decreased by around 4% from 5.18 g/cm<sup>3</sup> to 4.97 g/cm<sup>3</sup> for all instances.

### 3.2. Thermophysical properties

The most important thermophysical properties for the TES materials are the heat capacity, thermal conductivity and density [25–28].

Thermal conductivity and diffusivity obtained from the LFA measurements are presented in Fig. 4. The calculated thermal conductivity for the 1 day – 1000 °C treated Magnetite as bulk piece (Magnetite 1000-1) is very high. The obtained values are strongly above the average compared to other not rare low cost ceramic materials reported to have potential for TES applications [25–28]. The Magnetite thermal conductivity value is more than 2 times higher compared to ceramic materials considered for sensible TES like concrete, granite, marble, sandstone, etc [26], while its cost is less than 0.18 \$/kg [33], which can be considered slightly more expensive compared to concrete [25,28] or some by-products [27].

It can also be seen that thermal conductivity of raw Magnetite is in satisfactory agreement with the measurements of Noda et al. [34], considering that LFA is not a direct technique for thermal conductivity measurements and the fact that we use natural Magnetite, while a pure synthesized one was used in that reference. It is observed that the thermal diffusivity and the calculated thermal conductivity increase with the rising temperature of treatment of Magnetite approaching values which correspond to Hematite [34]. Such results suggest that higher temperature of treatment increases the fraction of Hematite in the sample since the values of thermal conductivity of the 1000 °C treated sample (Magnetite 1000-1) are much closer to Hematite than they are to Magnetite. It also gives the potential to reach the desired thermal conductivity for the material by varying the temperature of treatment (if material is used at non-oxidizing conditions). This could be an exceptional advantage for packed-bed systems, however, some additional expenses might be applied for high-temperature pretreatment depending on the particular application.

On the other hand, thermal diffusivity measurements clearly show a reversible phase transition at about 570 °C. The stored/released energy obtained by the endothermic/exothermic enthalpy of this reversible transformation may be very beneficial in the TES field.

Heat capacity measurements by DSC and LFA of the Magnetite 1000-1 (Fig. 5) (performed under Ar atmosphere) supports the presence of phase transition at the above-indicated temperature and are in excellent agreement with measurements presented in the

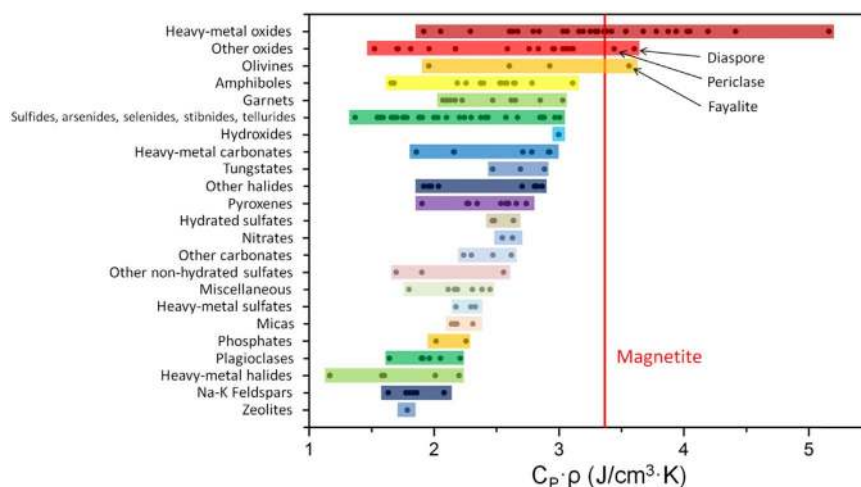


**Fig. 8.** Comparison of volumetric energy density of Magnetite with other minerals and nonporous rocks at 20 °C.

literature for Magnetite [35,36]. No noticeable (within the error of the measurement) effect of high temperature treatment on the heat capacity of the material was observed, which is in agreement with the fact that heat capacity of Magnetite and Hematite are nearly the same [35,36].

Such phase transition is related to antiferromagnetic transition of Magnetite [35] and is well repeatable.

Such a result suggest an opportunity to use the enthalpy of the indicated phase transition as latent TES in addition to the very attractive sensible TES characteristics of Magnetite (thermal conductivity, heat capacity and density).

It also raises the question regarding the stability of such phase transition, particularly partly because of the Magnetite to Hematite transformation. Therefore, 25 DSC cycles in a 50–725 °C temperature range were performed for raw Magnetite in the form of bulk piece (raw Magnetite) and powder (raw Magnetite-p) under air and argon atmospheres. For the bulk pieces, the results are similar for both air and argon atmospheres (Fig. 6): one endothermic reversible peak, for all the cycles, at about 570 °C with the enthalpy of  $17.9 \pm 0.4$  J/g is observed. Such a result suggests that there is negligible Magnetite to Hematite oxidation and the sample is mostly represented by the Magnetite. In order to check the case if such oxidation takes place during a practical application (for example due to longer operational time), contact area of the sample with air was increased by graining the raw Magnetite (Magnetite-p). In this case, the oxidation certainly takes place and two endothermic reversible peaks, for the 25th cycle, are observed at 570 and 690 °C which correspond to antiferromagnetic transition of Magnetite [35] and Hematite [37], respectively (Fig. 6b). LFA measurements for the Magnetite treated during 21 days at 1000 °C (Magnetite 1000-21) are also in favor of that transformation demonstrating two peaks for the calculated heat capacity (Fig. 7). The measurements in Fig. 7 should nevertheless be considered only as an indication of the presence of both transitions for Magnetite and Hematite, not for exact values the reason being that long time treatment of the material leads to its irreversible expansion of around 1% due to iron carbonate decomposition (0.1 wt% loss) and Magnetite to Hematite transformation (3 wt% gain, see Fig. 2a). Although such volume variation is rather small it results in non-uniform sample thickness, which is crucial for accuracy of LFA measurements. However, no cracks or fracture of the material were observed after the high temperature treatment.

Considering that the enthalpy of the discussed phase transitions for Magnetite and Hematite is almost the same, the capacity of latent heat stored upon the oxidation process is not lost, rather it shifts to a higher temperature. In order to prove this, additional DSC measurements for Magnetite 1000-p, which was confirmed by XRD to be completely

transformed to Hematite, were performed. Such measurements revealed the presence of only one peak at temperature of 690 °C with an enthalpy of  $20.1 \pm 0.5$  J/g. This indicates that independently on the transformation from Magnetite to Hematite the antiferromagnetic transition, which is known to be reversible [35,36], can be used with approximately the same enthalpy, except it will be proportionally distributed between the antiferromagnetic transitions of Magnetite (at 570 °C) and Hematite (at 690 °C) depending on their quantities present in the material.

Taking into account the reversible nature of the above described antiferromagnetic transition (Fig. 6), its enthalpy may be used as additional latent thermal energy. Compared to the enthalpies of phase change materials considered for latent TES [38,39], the registered enthalpy of antiferromagnetic transition of Magnetite is quite low. However, since this transition is not related to the aggregation state change it is an additional bonus for the use of Magnetite for thermal energy storage in sensible configuration. Apart from the attractive sensible TES characteristics, described phase transition adds additional latent thermal energy capacity to the material increasing its overall heat content.

Calculations of volumetric energy density ( $E = \rho \cdot c_p$ ) based on the measured values of heat capacity and density are presented in Fig. 5 (right side axis). Both  $c_p$  and  $E$  values demonstrate very good thermal energy storage capacity which is strongly above average compared with other materials for TES applications [25–28]. Detailed comparison with other minerals and nonporous rocks is presented in Fig. 8 using data gathered by Waples and Waples [40].

From Fig. 8, it is apparent that Magnetite is among the best performing materials (even without taking into account the enthalpy of antiferromagnetic transition in case of using this material at temperatures lower than the phase transition one), especially if one does not consider heavy-metal oxides for the comparison (for environmental reasons). There are very few materials exceeding Magnetite's energy density, namely Diaspore, Periclaste and Fayalite, which are much more rare compared to Magnetite.

From the obtained result Magnetite appears to be very interesting for TES, however, both mechanical and thermal stability as well as corrosion aspects must be considered in detail for each particular application conditions which will be the topic of upcoming case study works. At this point, some preliminary results have been presented in [41], where Magnetite was already tested for its compatibility with two heat transfer fluids, namely Delco Term mineral oil and HitecXL molten salt. In this work, the compatibility of Magnetite in direct contact with both HTFs up to 1500 h at 310 °C, the maximum operation temperature considered within the ORC-PLUS project [42], was demonstrated. As a next step of proposed material justification for

TES applications its stability will be investigated in terms of corrosion aspects and effect of operational conditions on mechanical properties within the framework of case studies investigations.

#### 4. Conclusions

A natural Magnetite was characterized and evaluated as a potential material for efficient thermal energy storage applications. A simple route consisting of temperature treatment of as-received material was proposed to partially transform Magnetite to Hematite and, as a result, take advantage of its excellent thermophysical properties, latent heat of reversible antiferromagnetic transition and ability to program thermal conductivity in case material is used under non-oxidation conditions (oil or CO<sub>2</sub> is used as HTF, for example). The possibility to control the thermal conductivity is an exceptional advantage for applications where certain optimal values are required, like packed-bed heat storage systems. Overall, thermal conductivity and volumetric energy capacity are strongly above average compared to reported materials for TES applications and are among the best ones if availability will be taken into account. Considering that such characteristics and properties are obtained for a material with low cost, abundant, high-melting temperature, ecological friendliness and non-flammability, we consider natural Magnetite and proposed treatment route as extremely promising for thermal energy storage applications, particularly for CSP plants having packed-bed storage configuration.

#### Acknowledgements

The authors acknowledge the financial support from the European Community through the H2020 program under Grant agreement number 657690. The authors express their sincere thanks to Naira Soguero Pérez and Ibai Intxaurreondo for their technical support. The help of Dr. Damien Saurel with PPMS measurements is also highly appreciated.

#### References

- [1] A.A. Mills, The lodestone: history, physics, and formation, *Ann. Sci.* 61 (2004) 273–319.
- [2] J. Roger, J.N. Pons, R. Massart, A. Halbreich, J.C. Bacri, Some biomedical applications of ferrofluids, *Eur. Phys. J. Appl. Phys.* 5 (1999) 321–325.
- [3] S. Oswald, W. Kinzelbach, A. Greiner, G. Brix, Observation of flow and transport processes in artificial porous media via magnetic resonance imaging in three dimensions, *Geoderma* 80 (1997) 417–429.
- [4] D.K. Kim, Y. Zhang, J. Kehr, T. Klason, B. Bjelke, M. Muhammed, Characterization and MRI study of surfactant-coated superparamagnetic nanoparticles administered into the rat brain, *J. Magn. Magn. Mater.* 225 (2001) 256–261.
- [5] A. Jordan, R. Scholz, P. Wust, H. Fähling, R. Felix, Magnetic fluid hyperthermia (MFH): cancer treatment with AC magnetic field induced excitation of biocompatible superparamagnetic nanoparticles, *J. Magn. Magn. Mater.* 201 (1999) 413–419.
- [6] R. Hiergeist, W. Andrä, N. Buske, R. Hergt, I. Hilger, U. Richter, W. Kaiser, Application of Magnetite ferrofluids for hyperthermia, *J. Magn. Magn. Mater.* 201 (1999) 420–422.
- [7] A. Navrotsky, L. Mazeina, J. Majzlan, Size-driven structural and thermodynamic complexity in iron oxides, *Science* 319 (2008) 1635–1638.
- [8] R.Y. Hong, T.T. Pan, H.Z. Li, Microwave synthesis of magnetic Fe<sub>3</sub>O<sub>4</sub> nanoparticles used as a precursor of nanocomposites and ferrofluids, *J. Magn. Magn. Mater.* 303 (2006) 60–68.
- [9] L. Blaney, Magnetite (Fe<sub>3</sub>O<sub>4</sub>): properties, synthesis, and applications, *Lehigh Preserv.* 15 (2007).
- [10] Ibrahim Dincer, Marc Rosen, *Thermal Energy Storage: Systems and Applications*, John Wiley & Sons, Chichester, England, 2002.
- [11] J.E. Pacheco, S.K. Showalter, W.J. Kolb, Development of a molten-salt thermocline thermal storage system for parabolic trough plants, *J. Sol. Energy Eng.* 124 (2002) 153–159.
- [12] D. Laing, W. Steinmann, R. Tamme, C. Richter, Solid media thermal storage for parabolic trough power plants, *Sol. Energy* 80 (2006) 1283–1289.
- [13] D. Laing, W.-D. Steinmann, M. Fib, R. Tamme, T. Brand, C. Bahl, Solid media thermal storage development and analysis of modular storage operation concepts for parabolic trough power plants, *J. Sol. Energy Eng.* 130 (2008) 11006.
- [14] C. Li, J. Ouyang, H. Yang, Novel sensible thermal storage material from natural minerals, *Phys. Chem. Miner.* 40 (2013) 681–689.
- [15] M. Cascetta, et al., A comparison between CFD simulation and experimental investigation of a packed-bed thermal energy storage system, *Appl. Therm. Eng.* 98 (2016) 1263–1272.
- [16] R. Anderson, S. Shirai, H. Bindra, J.F. Morris, Experimental results and modeling of energy storage and recovery in a packed bed of alumina particles, *Appl. Energy* 119 (2014) 521–529.
- [17] G. Zanganeh, A. Pedretti, S. Zavattini, M. Barbato, A. Steinfeld, Packed-bed thermal storage for concentrated solar power—Pilot-scale demonstration and industrial-scale design, *Sol. Energy* 86 (2012) 3084–3098.
- [18] M. Hänchen, S. Brückner, A. Steinfeld, High-temperature thermal storage using a packed bed of rocks—heat transfer analysis and experimental validation, *Appl. Therm. Eng.* 31 (2011) 1798–1806.
- [19] Z. Yang, S.V. Garimella, Thermal analysis of solar thermal energy storage in a molten-salt thermocline, *Sol. Energy* 84 (2010) 974–985.
- [20] A. Mawire, M. McPherson, Experimental and simulated temperature distribution of an oil-pebble bed thermal energy storage system with a variable heat source, *Appl. Therm. Eng.* 29 (2009) 1086–1095.
- [21] H.P. Garg, S.C. Mullick, V.K. Bhargava, *Solar Thermal Energy Storage*, Springer Science & Business Media, 2012.
- [22] A. Sharma, V.V. Tyagi, C.R. Chen, D. Buddhi, Review on thermal energy storage with phase change materials and applications, *Renew. Sustain. Energy Rev.* 13 (2009) 318–345.
- [23] M. Liu, N.H.S. Tay, S. Bell, M. Belusko, R. Jacob, G. Will, W. Saman, F. Bruno, Review on concentrating solar power plants and new developments in high temperature thermal energy storage technologies, *Renew. Sustain. Energy Rev.* 53 (2016) 1411–1432.
- [24] C. Xu, Z. Wang, Y. He, X. Li, F. Bai, Sensitivity analysis of the numerical study on the thermal performance of a packed-bed molten salt thermocline thermal storage system, *Appl. Energy* 92 (2012) 65–75.
- [25] S. Khare, M. Dell'Amico, C. Knight, S. McGarry, Selection of materials for high temperature sensible energy storage, *Sol. Energy Mater. Sol. Cells* 115 (2013) 114–122.
- [26] G. Li, Sensible heat thermal storage energy and exergy performance evaluations, *Renew. Sustain. Energy Rev.* 53 (2016) 897–923.
- [27] M.E. Navarro, M. Martínez, A. Gil, A.I. Fernández, L.F. Cabeza, R. Olives, X. Py, Selection and characterization of recycled materials for sensible thermal energy storage, *Sol. Energy Mater. Sol. Cells* 107 (2012) 131–135.
- [28] A.I. Fernandez, M. Martínez, M. Segarra, I. Martorell, L.F. Cabeza, Selection of materials with potential in sensible thermal energy storage, *Sol. Energy Mater. Sol. Cells* 94 (2010) 1723–1729.
- [29] D ASTM, 4503-86 Stand. Pract. Dissolution Solid Waste by Lithium Metaborate Fusion, (n.d.), 1998.
- [30] R.L. Danley, New modulated DSC measurement technique, *Thermochim. Acta* 402 (2003) 91–98.
- [31] W.J. Parker, R.J. Jenkins, C.P. Butler, G.L. Abbott, Flash method of determining thermal diffusivity, heat capacity, and thermal conductivity, *J. Appl. Phys.* 32 (1961) 1679–1684.
- [32] W.J. Parker, R.J. Jenkins, C.P. Butler, G.L. Abbott, Flash method of determining thermal diffusivity, heat capacity, and thermal conductivity, *J. Appl. Phys.* 32 (1961) 1679–1684.
- [33] S. Seetharaman, A. McLean, R. Guthrie, S. Sridhar, *Treatise on Process Metallurgy*, Elsevier, Boston, 2013.
- [34] Y. Noda, K. Naito, The thermal conductivity and diffusivity of Mn<sub>x</sub>Fe<sub>3-x</sub>O<sub>4</sub> (0≤x≤1.5) from 200 K to 700 K, *熱測定* 5 (1978) 11–18.
- [35] F. Grönvold, A. Sveen, Heat capacity and thermodynamic properties of synthetic Magnetite (Fe<sub>3</sub>O<sub>4</sub>) from 300 K to 1050 K. Ferrimagnetic transition and zero-point entropy, *J. Chem. Thermodyn.* 6 (1974) 859–872.
- [36] B.S. Hemingway, Thermodynamic properties for bunsenite, NiO, Magnetite, Fe<sub>3</sub>O<sub>4</sub>, and hematite, Fe<sub>2</sub>O<sub>3</sub>, with comments on selected oxygen buffer reactions, *Am. Mineral.* 75 (1990) 781–790.
- [37] J. Lielmezs, A.C.D. Chaklader, Reversible thermal effect in α-Fe<sub>2</sub>O<sub>3</sub> at 690 ± 5 C, *J. Appl. Phys.* 36 (1965) 866.
- [38] M.M. Kenisarin, Thermophysical properties of some organic phase change materials for latent heat storage. A review, *Sol. Energy* 107 (2014) 553–575.
- [39] B. Xu, P. Li, C. Chan, Application of phase change materials for thermal energy storage in concentrated solar thermal power plants: a review to recent developments, *Appl. Energy* 160 (2015) 286–307.
- [40] D.W. Waples, J.S. Waples, A review and evaluation of specific heat capacities of rocks, minerals, and subsurface fluids. Part 1: minerals and nonporous rocks, *Nat. Resour. Res.* 13 (2004) 97–122.
- [41] Y. Grosu, I.Ortega-Fernández, A.Faik, K.Mani, B.D'Aguanno, Corrosion study for different sensible heat storage materials and heat transfer fluids. SolarPACES 2016, Abu Dhabi, United Arab Emirates, 2016, pp. 11–14.
- [42] (<http://www.orc-plus.eu/>)